Polarization Changes in Optical Fibers induced by Self-Phase Modulation and Cross-Phase Modulation in Conjunction with Birefrigence

Lutz Rapp

Polarization Changes in Optical Fibers induced by Self–Phase Modulation and Cross–Phase Modulation in Conjunction with Birefrigence

Lutz Rapp

July 20, 2008

Abstract— **Polarization dependence of various fiber effects affecting signal quality in wavelength division multiplexing (WDM) systems has become a major field of research activities. Polarization–mode dispersion (PMD) and polarization–dependent loss (PDL) are quite well understood today, but there are still major open questions with respect to the interaction with nonlinear fiber effects, although the picture has already become clearer. The aim of this paper is to provide a better understanding of the impact of self–phase modulation (SPM), cross–phase modulation (XPM), and birefrigence on the state of polarization during propagation in a transmission fiber. For several configurations, closed–form expressions describing the dependence of different quantities on propagation distance are presented.**

Both phase modulating effects do not induce a power transfer among the channels of WDM system. However, power is exchanged among the components of the Jones vector of the individual channels. Without attenuation, this power exchange is a periodic function of the propagation distance. Furthermore, the analysis reveals that the sum of the ellipticities weighted by the corresponding fiber input power is preserved during propagation as long as the wavelength dependence of fiber attenuation can be neglected.

In the presence of SPM only, the ellipticity of the channel under consideration is maintained during propagation and the powers of the different components of the Jones vector change sinusoidally as a function of a normalized propagation distance. Closed–form expressions describing the dependence of the magnitude of the power variation and the period length on initial conditions at the fiber input are derived. Conservation of the ellipticity is canceled out by the interaction with birefrigence. Neglecting fiber attenuation, a different quantity is identified that is conserved during propagation. Ellipticity as well as the power of the two components of the Jones vector change periodically versus propagation distance, but no longer sinusoidally. Furthermore, it is shown that there is a separatrix that cannot be crossed by the traces embracing the states of polarization adopted during propagation. Thus, the Poincaré sphere is split into up to three segments.

The ellipticity of a channel influenced by XPM has a sinusoidal dependence on the normalized propagation distance with a period length depending on the ellipticity of the first channel only. Power variation of both components of the Jones vector of the second channel can be mathematically described by a superposition of three sine waves. The magnitude of the power exchange on initial conditions at the fiber input is pointed out. In addition, this analysis is extended for the case that a channel is affected by SPM, XPM, and birefrigence simultaneously.

Index Terms— **Optical communications, optical networks, wavelength division multiplexing, self–phase modulation, cross–phase modulation, birefrigence, polarization–mode dispersion, state of polarization**

This work has been done at the Communication Technology Laboratory, Swiss Federal Institute of Technology (ETH), Zurich, Switzerland, in 1996. It has now been updated and translated into English.

I. Introduction

SINGLE–mode fibers, also called monomode fibers, are the only kind of transmission medium used today for long–haul communications. The name of these fibers suggests that they support the propagation of a single fundamental mode only [1]. But in fact, there are two modes of propagation [2] which are mutually orthogonally polarized. Under weakly guiding conditions, they can be assumed to be linearly polarized. In an ideal cylindrical waveguide, these two modes are degenerate, which means, that there is no difference between their propagation constants. Thus, they propagate with the same phase–velocity.

Real fibers are neither completely circular nor perfectly straight. In addition, the fiber material is slightly anisotropic. As a consequence, the propagation constants of the two modes becomes different, which is referred to as birefrigence [3]. The axis with maximum propagation velocity is called fast axis, whereas the axis with minimum propagation velocity is named slow axis. Birefrigence leads to a periodic change of the state of polarization during propagation. Furthermore, fiber employed in field environments are exposed to mechanical stress, temperature variation, twists and bends [4] causing unstable fluctuations in the polarization state of the propagating light.

Random variations of birefrigence give rise to effects summarized under the term polarization–mode dispersion (PMD) [5]. The interest in these effects has grown with increasing bitrate of the transmitted wavelength division multiplexing (WDM) channels. In particular when using older fibers, PMD may become one of the most serious impairments in high–bitrate system. Not surprisingly, the impact of PMD on system performance has been studied widely [6]. As an example, quite early results on optical transmission system penalties are described in [7]. A large number of concepts to compensate or at least to reduce the impact of these effects have been developed in the last years [8][9]. Polarization–dependent loss

(PDL) or gain (PDG) [10] is another effect related to the state of polarization that may affect system performance.

Nonlinear fiber effects constitute another class of effects having the potential to severely degrade signal quality. Performance degradation caused by self–phase modulation (SPM) [11][12] and four–wave mixing (FWM)[13] has been investigated from the beginning of the commercial deployment of WDM systems, both, theoretically and experimentally. However, the effect of cross–phase modulation (XPM) has been overlooked for a while [14]. Although the influence of polarization was apparent from some early experiments [15], polarization has either been completely neglected in theoretical investigations [16] or only worst case situations have been considered [17] for several years.

Already in 1995, it has been shown that performance degradation resulting from PMD can be mitigated by means of the Kerr effect for nonreturn–to–zero signals [18]. Since around 1999, the interaction of PMD with nonlinear fiber effects is investigated more thoroughly.

Many of the investigations are devoted to XPM and degradation of the degree of polarization (DOP). It has been shown experimentally that, from a statistical point of view, PMD is exacerbated in presence of XPM, as long as polarization interleaving is not employed. In addition, XPM–induced depolarization can lead to a degradation of PMD compensator efficiency [19][20]. A closed–form approximate expression for DOP degradation of a signal degraded by XPM of a nonlinearly interfering pump is presented in [21]. Furthermore, it turned out that channel depolarization occurs on a time scale comparable with the bit period [22].

Significant progresses have also been achieved in the field of modeling the interaction of PMD with nonlinearity. Fundamental aspects are reviewed in a tutorial [23] with focus on the derivation the Manakow equation. A vector theory of XPM in optical fibers has been developed [24][25] that is mainly useful for pump–probe configurations and allowed to derive an analytical expression for the amplitude of probe fluctuations by a copropagating pump channel. In addition, the theory revealed that PMD helps to reduce the XPM–induced crosstalk in WDM systems, as long as polarization interleaving is not used. This result is in good agreement with findings based on system simulations and laboratory experiments [26], leading to the statement, that evaluations making use of the scalar nonlinear Schrödinger equation tend to overestimate the XPM interchannel coupling of WDM transmission. Models including the effect of FWM are also available [27]. In a pump–probe configuration, states of polarization different from the carrier have been observed for optical spectral components generated by XPM [28].

In presence of large dispersion, the mean field approach is useful [29]. It provides results with sufficient accuracy at significantly reduced computational effects as compared with techniques based on the Manakov equation. The calculations are based on the Stokes parameters of the WDM channels only and they ignore the detailed temporal behavior when determining the evolution of the polarization.

First, different representations used to illustrate the evolution of the state of polarization are described. Next, a mathematical description is presented and some fundamental properties of the evolution of the state of polarization are derived. In section IV, the effect of self–phase modulation on the state of polarization is investigated, whereas its interaction with birefrigence is considered in section V. Section VI deals with the effect of XPM and its interplay with SPM. Subject of section VII is the interaction of XPM with birefrigence. Finally, the results are summarized and some conclusions are drawn.

II. Representation of states of polarization

Light phenomena in optical fibers can be described by using the notion of electromagnetic fields propagating as transverse waves [30]. Conventionally, when considering polarization, the electric field vector is described only, since the magnetic field is perpendicular to the electric field and the amplitudes of both fields are proportional to each other.

Any arbitrary state of polarization can be created by superimposing two linearly polarized waves, which are oriented in orthogonal directions of a Cartesian coordinate system. For a simple harmonic wave, where the amplitude of the electric vector varies in a sinusoidal manner, the two components have exactly the same frequency. In general, the amplitude and the phase of these waves are different.

Typically, a right–oriented coordinate system is used to describe the propagation of a lightwave in an optical fibers, where the z–axis is oriented in the direction of propagation. Thus, polarized light can be represented by a two–element complex vector, the elements of which represent the complex envelopes of the two linearly polarized waves. This so called Jones vector has the form

$$\begin{aligned}\vec{E}_{\text{ell}} &= E_0 \begin{bmatrix} u_x \\ u_y \end{bmatrix} = E_0 \begin{bmatrix} \xi_x \cdot e^{\jmath\varphi_x} \\ \xi_y \cdot e^{\jmath\varphi_y} \end{bmatrix} \\ &= E_0 \cdot e^{\jmath\varphi_x} \begin{bmatrix} \xi_x \\ \sqrt{1-\xi_x^2} \cdot e^{\jmath\Delta\varphi} \end{bmatrix} \end{aligned} \quad (1)$$

with $0 \leq \xi_x \leq 1$ and $\Delta\varphi = \varphi_y - \varphi_x$. All parameters on the right side of the last equal sign represent real quantities. The real quantity E_0 represents the magnitude of the electrical field vector, whereas the complex quantities u_x and u_y are normalized complex envelopes with $|u_x|^2 + |u_y|^2 = 1$. The variables φ_x and φ_y stand for the respective phase terms.

The pattern traced out by the electrical field has elliptical shape. In general, the principal axes of the ellipse are tilted against the x–axis and the y–axis. The angle between the x–axis and the larger principal axis of the ellipse will be denoted by α_{rot} in the following, as shown in Fig. 1. Another important parameter characterizing the polarization ellipse is the ellipticity

$$\epsilon = 2 \cdot \xi_x \cdot \sqrt{1-\xi_x^2} \cdot \sin(\Delta\varphi) \quad . \quad (2)$$

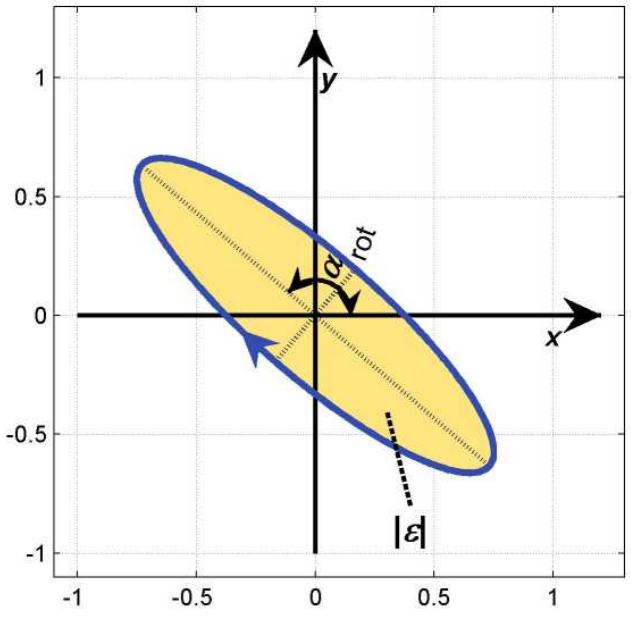

Fig. 1. Schematic representation of the polarization ellipse.

The magnitude of this parameter indicates the size of the area covered by the ellipse, whereas the sign of this parameter specifies the sense of rotation of the electrical field vector. Positive numbers indicate that the field vector is rotating clockwise as seen by an observer from whom the wave is moving away ($0° \leq \Delta\varphi < 180°$), whereas the electric field is rotating counter clockwise if the parameter value is negative ($180° \leq \Delta\varphi < 360°$).

Stokes parameters constitute another common way to describe the state of polarization of a lightwave. For the following consideration, the three standard Stokes parameters

$$S_1 = 2 \cdot \xi_x^2 - 1 \quad (3)$$

$$S_2 = 2 \cdot \xi_x \cdot \sqrt{1-\xi_x^2} \cdot \cos(\Delta\varphi) \quad (4)$$

$$S_3 = 2 \cdot \xi_x \cdot \sqrt{1-\xi_x^2} \cdot \sin(\Delta\varphi) = \epsilon \quad (5)$$

with

$$S_1^2 + S_2^2 + S_3^2 = 1 \quad (6)$$

are sufficient. The parameter S_3 is identical to the already introduced ellipticity ϵ.

Commonly, the state of polarization of a lightwave is represented on the Poincaré sphere. However, this three dimensional representation does not always reveal clearly all important features. Therefore, two additional kinds of representation will be used. Both make use of polar coordinates. One of them is directly based on the Jones representation of the state of polarization and can always be found on the right side of figures describing the state of polarization. The radius is identified with the parameter ξ_x and the angle with reference to the x–axis corresponds to $\Delta\varphi$. As shown by the template in Fig. 2, all linear states of polarization are found on the x–axis, whereas the data points $(0, \sqrt{2})$ and $(0, -\sqrt{2})$ represent

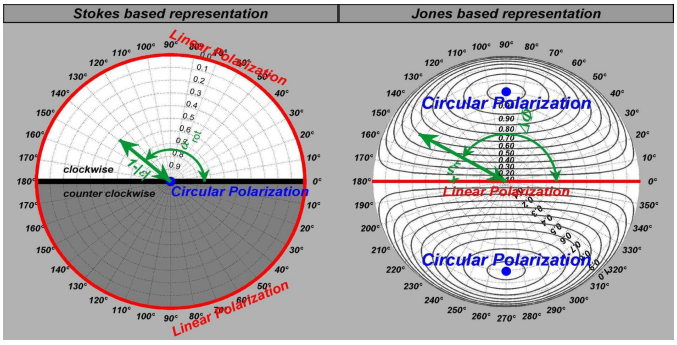

Fig. 2. Stokes and Jones based representation of polarization states.

circular states of polarization. Traces with constant magnitude of the ellipticity have been marked by closed curves.

Representations on the left side of the figures are related to the Stokes representation. In this case, the angle with reference to the x–axis in the plot indicates the rotation of the transverse axis of the polarization axis, whereas the radius is a function of the magnitude of the ellipticity and is given by $r = 1 - |\epsilon|$. Thus, linear states of polarization are located on the outer circle with radius one and circular polarization is found at the origin or coordinates. In both representations, clockwise rotating states of polarization are found in the upper half–plane, whereas the lower half–plane comprises all states of polarization with counter clockwise rotation.

III. Mathematical Description

Let us consider a wavelength division multiplexing system with N channels. Since arbitrary elliptical polarizations are allowed, two linear lightwaves with orthogonal polarizations have to be considered per channel. In total, there are $2N$ lightwaves propagating within the optical fiber.

Four–wave mixing (FWM) is an important effect causing interaction between different channels transmitted simultaneously in an optical fiber. However, this effect is only effective if the phase matching condition is fulfilled. Therefore, it is generally assumed that this effect can be neglected in standard single–mode fibers (SSMFs) due to their large dispersion leading to phase mismatch already at quite small channels spacings.

In the present case, there is a complementary lightwave to each lightwave having the same wavelength. Therefore, phase matching occurs for some of the four–wave mixing products despite the large dispersion, as long as this is not prevented by birefrigence or polarization mode dispersion (PMD). In the following, we will limit our investigations to fibers having large dispersion, so that only four–wave mixing mediated interaction among lightwaves having identical wavelengths plays an important role.

The mathematical description of the wave propagation within the optical fiber is based on Cartesian coordinates. The axis of propagation coincides with the z–axes. The temporal and spatial evolution of the complex envelope is characterized

by the normalized parameters $u_{xi}(\tau, z)$ and $u_{yi}(\tau, z)$, respectively. In addition, it is assumed that lightwaves with the same frequency have identical modal field distribution. Furthermore, the typically small wavelength dependence of attenuation is neglected. This assumptions lead to the system of differential equations (7)[1]. Due to space limitations, the dependence of the different parameters on time and space is not indicated explicitly. Average power levels of the different channels at the fiber input are denoted by P_i and P_j, respectively. The parameters β_i stem from an expansion of the mode–propagation constant β in a Taylor series about the center frequency. The extent of nonlinear fiber effects is governed by the nonlinear–index coefficient n_2 [31].

Typically, all channels are located within one transmission window of the optical fiber. Thus, the difference with respect to the modal field distributions are small and the overlap integrals g_{ii} and g_{ij}, respectively, can be assumed to be constant and can be replaced by the inverse of the effective area A_{eff}. Replacing the individual wavelengths λ_i and λ_j by the average wavelength $\bar{\lambda}$ allows to introduce a normalized effective length

$$\begin{aligned} \zeta &= 2\pi \frac{n_2 P_0}{\bar{\lambda} A_{\text{eff}}} \frac{1}{\alpha} \left[1 - \exp\left(-\alpha z\right) \right] \\ &= \frac{1}{z_{\text{eff}}} \frac{1}{\alpha} \left[1 - \exp\left(-\alpha z\right) \right] \end{aligned} \tag{8}$$

with

$$z_{\text{eff}} = \frac{\bar{\lambda} A_{\text{eff}}}{2\pi n_2 P_0} \quad .$$

The parameter P_0 denotes an arbitrary power level greater than zero. It is a good choice to set this parameter value to the maximum channel power at the fiber input. Please note that the parameter ζ tends towards a finite value

$$\zeta_{\text{max}} = \frac{1}{z_{\text{eff}} \cdot \alpha} \tag{9}$$

when increasing the coordinate z continuously in the presence of fiber attenuation ($\alpha > 0$). As a consequence, the range of values of ζ is limited to the interval $[0\, \zeta_{\text{max}}]$.

For the following investigations on polarization changes induced by nonlinear fiber effects, it will be assumed that the complex envelopes of the electrical field are time independent. Changes of the amplitude and phase of the complex envelope are described by separate differential equations. Since the state of polarization depends on the phase difference between the two components u_{xi} and u_{yi} only, the propagation of all lightwaves within the transmission fiber can be described by $3N$ coupled differential equations containing real numbers only. The resulting system of coupled differential equations is given by (10). It follows from the first two equations that the sum $\xi_{xi}^2 + \xi_{yi}^2$ is constant during propagation.

[1]In this work, the propagation of a plane wave with wave vector $\vec{k}$ is described by the term $\exp\left\{ \jmath \left(\Omega \cdot \tau - \vec{k} \cdot \vec{r} \right) \right\}$, where $\vec{r}$ stands for the position vector and Ω denotes the angular frequency. When using the complete conjugate description, as done in [31], the sign of terms with leading imaginary symbol changes.

Self–phase modulation and cross–phase modulation do not induce power exchange among the different channels of a WDM system, but power is exchanged between the two components of the Jones vectors of the channels.

From the already mentioned set of differential equations (10) with real quantities, an additional equation can be derived for the ellipticity of the lightwaves:

$$\begin{aligned} &\frac{\partial}{\partial \zeta} \left\{ 2\xi_{xi} \sqrt{1 - \xi_{xi}^2} \sin\left(\Delta\varphi_i\right) \right\} \\ &= \frac{8}{3} \sum_{j \neq i} \frac{P_j}{P_0} \Bigg[\left(1 - 2\xi_{xi}^2\right) \xi_{xj} \sqrt{1 - \xi_{xj}^2} \cos\left(\Delta\varphi_j\right) \\ &\qquad - \left(1 - 2\xi_{xj}^2\right) \xi_{xi} \sqrt{1 - \xi_{xi}^2} \cos\left(\Delta\varphi_i\right) \Bigg] \end{aligned} \tag{11}$$

Weighting the ellipticity of all channels with the corresponding fiber input powers and summing up all these terms leads to an additional figure that is preserved during propagation.

$$\begin{aligned} &\sum_{i=1}^{N} \frac{P_j}{P_0} \cdot 2\xi_{xi} \sqrt{1 - \xi_{xi}^2} \sin\left(\Delta\varphi_i\right) \\ &\qquad = \sum_{i=1}^{N} \frac{P_j}{P_0} \cdot \epsilon_i = \text{const.} \end{aligned} \tag{12}$$

The sum of ellipticities weighted by the corresponding fiber input power is preserved during propagation.

In the following, the powers $\mathcal{P}_{xi} = \xi_{xi}^2$ of the waves that are linearly polarized in direction of the x–axis will be used instead of the amplitudes ξ_{xi}.

For interpretation of the results presented in the following, it is of importance to be aware of the effect of birefrigence on polarization. Fig. 3 shows closed curves representing traces of the state of polarization that are adopted during propagation due to birefrigence in a fiber without nonlinearity. In the Jones based representation, we get circles that are centered at the origin of the system of coordinates. The Stokes based representation indicates that the magnitude of the ellipticity changes almost continuously. In addition, the curves are symmetrical with respect to the x–axis and the y–axis. The important point is that significant parts of the curves can be approximated by straight lines. Thus, we can describe the behavior qualitatively by stating that the orientation of the polarization ellipse switches between two directions. The angle with the x–axis corresponds either to its initial value α_{init} at the fiber input or to $180° - \alpha_{\text{init}}$.

Remark: *It is common practice to denote all nonlinear interactions between polarization components of one channel by SPM. However, this wording is not correct in a strict sense since the nonlinear effects do no only induce modulation of*

$$\begin{aligned}
\frac{\partial u_{xi}}{\partial z} &+ \Delta\beta_1(\lambda_i)\frac{\partial u_{xi}}{\partial \tau} - \jmath\frac{\beta_2(\lambda_i)}{2}\frac{\partial^2 u_{xi}}{\partial \tau^2} - \frac{\beta_3(\lambda_i)}{6}\frac{\partial^3 u_{xi}}{\partial \tau^3} \\
&= -\jmath\frac{2\pi n_2}{\lambda_i}\exp(-\alpha z)\left\{ g_{ii}P_i u_{xi}\left[|u_{xi}|^2 + \frac{2}{3}|u_{yi}|^2\right] + \frac{1}{3}g_{ii}P_i u_{xi}^* u_{yi}^2 \right. \\
&\qquad \left. + \sum_{j\neq i}^{N} g_{ij}P_j u_{xi}\left[2|u_{xj}|^2 + \frac{2}{3}|u_{yj}|^2\right] + \frac{2}{3}\sum_{j\neq i}^{N} g_{ij}P_j u_{yi}\left[u_{xj}u_{yj}^* + u_{xj}^* u_{yj}\right] \right\} \\
\frac{\partial u_{yi}}{\partial z} &+ \Delta\beta_1(\lambda_i)\frac{\partial u_{yi}}{\partial \tau} - \jmath\frac{\beta_2(\lambda_i)}{2}\frac{\partial^2 u_{yi}}{\partial \tau^2} - \frac{\beta_3(\lambda_i)}{6}\frac{\partial^3 u_{yi}}{\partial \tau^3} \\
&= -\jmath\frac{2\pi n_2}{\lambda_i}\exp(-\alpha z)\left\{ g_{ii}P_i u_{yi}\left[|u_{yi}|^2 + \frac{2}{3}|u_{xi}|^2\right] + \frac{1}{3}g_{ii}P_i u_{yi}^* u_{xi}^2 \right. \\
&\qquad \left. + \sum_{j\neq i}^{N} g_{ij}P_j u_{yi}\left[2|u_{yj}|^2 + \frac{2}{3}|u_{xj}|^2\right] + \frac{2}{3}\sum_{j\neq i}^{N} g_{ij}P_j u_{xi}\left[u_{yj}u_{xj}^* + u_{yj}^* u_{xj}\right] \right\} \qquad (7)
\end{aligned}$$

$$\begin{aligned}
\frac{\partial \xi_{xi}}{\partial \zeta} &= \frac{1}{3}\left\{ \left[\frac{P_i}{P_0}\right]\xi_{xi}\xi_{yi}^2 \sin(2\Delta\varphi_i) + 4\xi_{yi}\sin(\Delta\varphi_i)\sum_{j\neq i}\left[\frac{P_j}{P_0}\right]\xi_{xj}\xi_{yj}\cos(\Delta\varphi_j) \right\} \\
\frac{\partial \xi_{yi}}{\partial \zeta} &= -\frac{1}{3}\left\{ \left[\frac{P_i}{P_0}\right]\xi_{yi}\xi_{xi}^2 \sin(2\Delta\varphi_i) + 4\xi_{xi}\sin(\Delta\varphi_i)\sum_{j\neq i}\left[\frac{P_j}{P_0}\right]\xi_{xj}\xi_{yj}\cos(\Delta\varphi_j) \right\} \\
\frac{\partial \Delta\varphi_i}{\partial \zeta} &= -\frac{1}{3}\left\{ \left[\frac{P_i}{P_0}\right]\left(\xi_{yi}^2 - \xi_{xi}^2\right)(1-\cos(2\Delta\varphi_i)) + 4\sum_{j\neq i}\left[\frac{P_j}{P_0}\right]\left(\xi_{yj}^2 - \xi_{xj}^2\right) \right. \\
&\qquad \left. + 4\left[\frac{\xi_{xi}}{\xi_{yi}} - \frac{\xi_{yi}}{\xi_{xi}}\right]\cos(\Delta\varphi_i)\sum_{j\neq i}\left[\frac{P_j}{P_0}\right]\xi_{xj}\xi_{yj}\cos(\Delta\varphi_j) \right\} \qquad (10)
\end{aligned}$$

the phase. There is a power exchange also in the absence of dispersion caused by degenerate FWM terms.

IV. The effect of self–phase modulation

In this section, the propagation of a single channel affected by self–phase modulation is considered. According to equation (12), the ellipticity $\varepsilon_1 = 2\xi_{x1}\sqrt{1-\xi_{x1}^2}\sin(\Delta\varphi_1)$ is maintained during propagation. With growing value of ζ, the state of polarization follows the curves shown in figure 4. The shape of the polarization ellipse as well as the sense of rotation of the electrical field vector remain unchanged, only the principal axes are rotated.

The power of the electrical field vector in direction of the x–axis as a function of the parameter ζ can be described analytically by

$$\mathcal{P}_{x1} = \frac{1}{2}\left[1 + \sqrt{1-\varepsilon_1^2}\cdot\sin\left(\frac{\zeta+\zeta_{01}}{\zeta_{c1}}\right)\right] \quad . \qquad (13)$$

Two new figures are introduced that depend on the initial condition at the fiber input as indicated by the following equations:

$$\begin{aligned}
\zeta_{c1} &= \frac{3}{2|\varepsilon_1|}\cdot\frac{P_0}{P_1} \\
\zeta_{01} &= \zeta_{c1}\cdot\arcsin\left(\frac{2\mathcal{P}_{x1}(0)-1}{\sqrt{1-\varepsilon_1^2}}\right) \qquad (14)
\end{aligned}$$

The normalized power of the component in direction of the x–axis has a sinusoidal dependence on the normalized distance ζ. The average value always equals $\frac{1}{2}$, irrespectively of the state of polarization at the fiber input. In contrast, the period

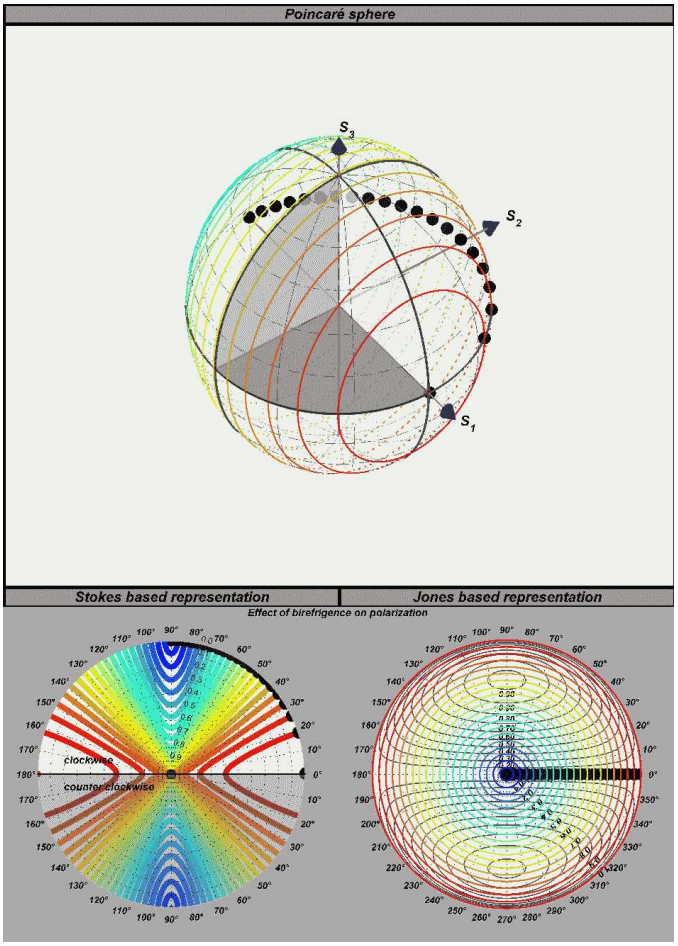

Fig. 3. Changes of the state of polarization induced by birefrigence.

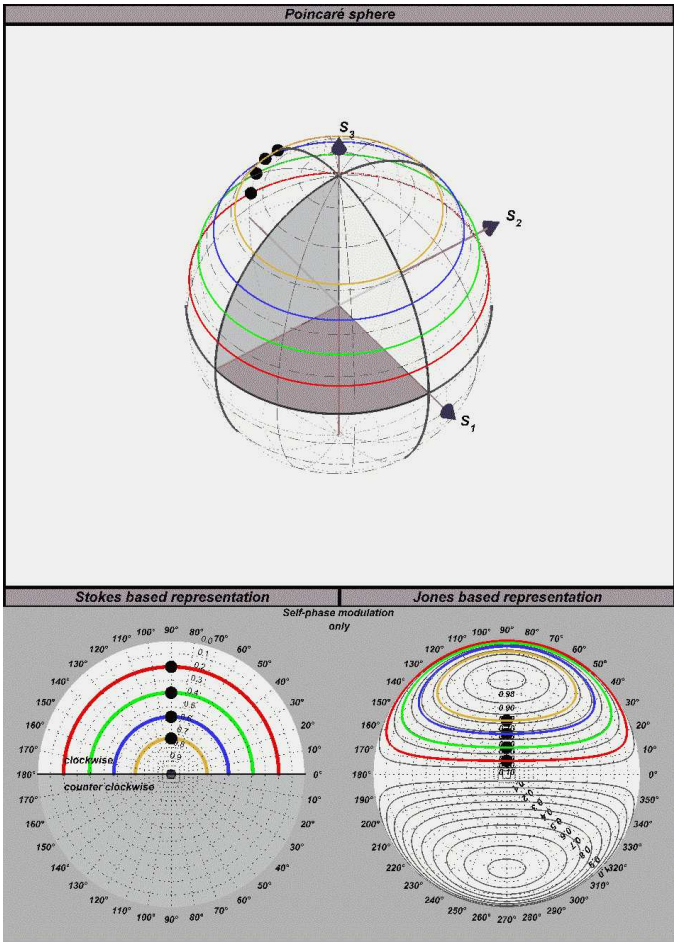

Fig. 4. Changes of the polarization state induced by self-phase modulation only. The polarization state at the fiber input has been marked by a dot.

length as well as the extent of the power exchange depend on the initial condition. Smaller magnitude of the ellipticity goes along with a larger period length and increasing extent of the power exchange. In the borderline case of linear polarization (vanishing ellipticity), the period length tends toward infinity, so that there is no power exchange.

Of particular interest are states of polarization that do not undergo changes during propagation. In the Jones based representation, this applies to all polarization states on the unit circle and all polarization states on the dividing line between upper and lower semicircle. By the way, this dividing line constitutes a separatrix, since all states of polarization that a lightwaves takes during propagation are either above of below this line. In addition, all points in this plane with a radius of $\frac{1}{\sqrt{2}}$ and a phase difference of $\pm 90°$ (circular polarization) are stationary.

In case of linear and circular polarization, self–phase modulation does not induce any change of the state of polarization. In addition, self–phase modulation alone does not induce changes of the sense of rotation of the electrical field vector.

In figure 5, the evolution of the power in the x–axis as well as the ellipticity are shown versus the normalized propagation distance ζ for the polarization states that have been marked by dots in figure 4.

V. Interplay of Self–Phase Modulation and Birefrigence

When considering the propagation of lightwaves with time independent complex envelopes of the electrical field, only differences with respect to the phase velocity are of importance. The different propagation constants can be taken into account by modifying the set of differential equations (7). The result

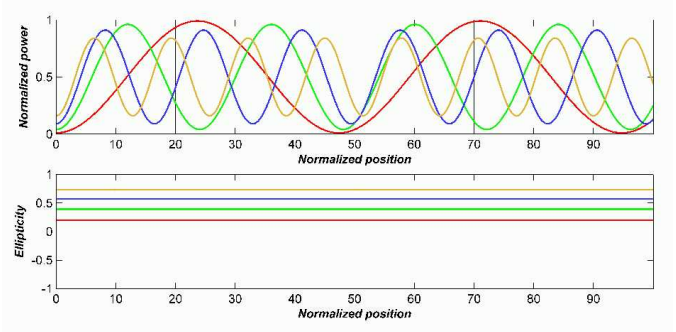

Fig. 5. Evolution of power in the x–axis and ellipticity versus normalized fiber position for different polarization states at the fiber input due to self–phase modulation (no birefrigence).

can be taken from (15). The parameter $\Delta\beta_i$ stands for the difference of the propagation constants for the two components of the Jones vector of channel i.

Again, it is helpful to describe changes of the magnitude of the complex parameters and their phase difference by separate differential equations. The resulting set of differential equations can be derived directly from (10) by replacing the last equation describing the evolution of the phase difference by equation (16).

A. *without attenuation*

First, the situation with vanishing attenuation is analyzed. In the Jones based representation and on the Poincaré sphere, we again get closed curves that are characterized by the equation

$$\frac{2}{3}\xi_x^2\left(1-\xi_x^2\right)\sin^2(\Delta\varphi)+\Delta\beta\cdot z_{\text{eff}}\cdot\xi_x^2 = \text{ const} \quad . \qquad (17)$$

This equation indicates that the quantity

$$\epsilon^2+6\Delta\beta\cdot z_{\text{eff}}\cdot\xi_x^2$$

is conserved during propagation. For different initial states of polarization but constant birefrigence, the closed curves are shown in figure 6. The power of the component in direction of the x–axis versus normalized propagation distance and the ellipticity along the fiber axis can be taken from figure 7.

As discussed before, self–phase modulation alone does not alter the ellipticity of a lightwave and induces a sinusoidal power exchange among the two elements of the Jones vector. The average power in directions of the x–axis and the y–axis equals $\frac{1}{2}$. Combined with birefrigence, there is still a periodic power exchange among the two element, but it is no longer sinusoidal and the average power values of the two powers are in general no longer equal, as shown in figure 9 for different values of the birefrigence. The ellipticity also shows a periodic behavior versus propagation distance. At small birefrigence, the sign of the ellipticity does not changes, which implies that the corresponding traces on the Poincaré sphere (see figure 8) are either completely in the lower or the upper hemisphere. In addition, the amount of the exchanged power as well as the period length of the power exchange increase with growing birefrigence until a certain value has been reached at which the trace of polarization states comprises states with positive and negative ellipticity. If the birefrigence is further increased, the amount of exchanged power as well as the period length decrease. In the borderline case of infinite birefrigence or infinite product $\Delta\beta\cdot z_{\text{eff}}$, the traces degenerate into circles in the Jones based representation or straight lines in the Stokes based representation. In addition, there is no power exchange anymore.

Whether the orientation of the rotation of the electrical field vector changes during propagation depends on the magnitude of the product $\Delta\beta\cdot z_{\text{eff}}$ and the state of polarization at the fiber input. For a given value of this product, we can distinguish between initial states of polarization that lead to a change of the sign of the ellipticity and states for which such a

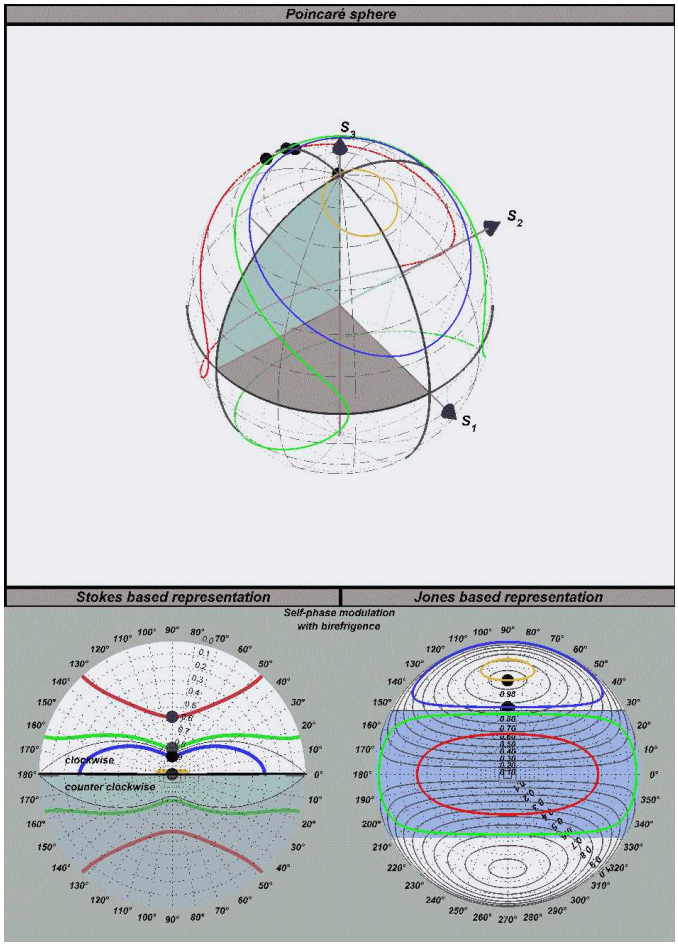

Fig. 6. Changes of the polarization state induced by self–phase modulation and birefrigence without fiber attenuation. The polarization state at the fiber input has been marked by a dot (constant birefrigence).

change does not happen. According to this criterion, the area containing all possible states of polarization in the Jones based representation can be segmented into different areas that are separated by separatrices. For the fast axis in direction of the x–axis, the separatrix is shown in Fig. 6 for $\Delta\beta\cdot z_{\text{eff}}=0.15$. In general, the separatrix is described by

$$\mathcal{P}_{sA}\cdot\sin^2(\Delta\varphi)=\frac{3}{2}\left|\Delta\beta\right| z_{\text{eff}} \quad ,$$

where $\mathcal{P}_{sA}=(1-\xi_{xi}^2)$ stand for the power in direction of the

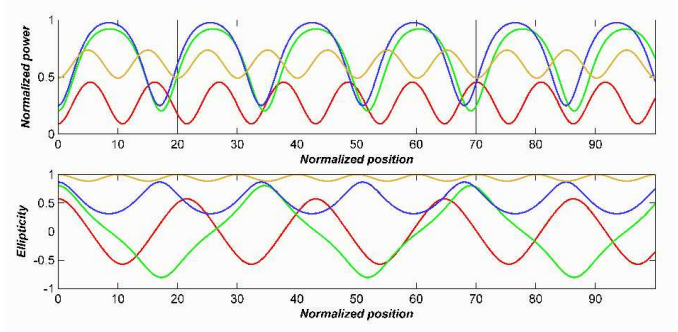

Fig. 7. Evolution of power in direction of the x–axis and ellipticity versus normalized fiber position for different polarization states at the fiber input (no fiber attenuation, with birefrigence).

$$\begin{aligned}
\frac{\partial u_{xi}}{\partial z} - \jmath\frac{\Delta\beta_i}{2}u_{xi} &= -\jmath\frac{2\pi n_2}{\lambda_i}\exp\left(-\alpha z\right)\left\{ g_{ii}P_i u_{xi}\left[|u_{xi}|^2 + \frac{2}{3}|u_{yi}|^2\right] + \frac{1}{3}g_{ii}P_i u_{xi}^* u_{yi}^2 \right. \\
&\quad \left. + \sum_{j\neq i}^{N} g_{ij}P_j u_{xi}\left[2|u_{xj}|^2 + \frac{2}{3}|u_{yj}|^2\right] + \frac{2}{3}\sum_{j\neq i}^{N} g_{ij}P_j u_{yi}\left[u_{xj}u_{yj}^* + u_{xj}^* u_{yj}\right] \right\} \\
\frac{\partial u_{yi}}{\partial z} + \jmath\frac{\Delta\beta_i}{2}u_{yi} &= -\jmath\frac{2\pi n_2}{\lambda_i}\exp\left(-\alpha z\right)\left\{ g_{ii}P_i u_{yi}\left[|u_{yi}|^2 + \frac{2}{3}|u_{xi}|^2\right] + \frac{1}{3}g_{ii}P_i u_{xi}^* u_{yi}^2 \right. \\
&\quad \left. + \sum_{j\neq i}^{N} g_{ij}P_j u_{yi}\left[2|u_{yj}|^2 + \frac{2}{3}|u_{xj}|^2\right] + \frac{2}{3}\sum_{j\neq i}^{N} g_{ij}P_j u_{xi}\left[u_{yj}u_{xj}^* + u_{yj}^* u_{xj}\right] \right\} \qquad (15)
\end{aligned}$$

$$\begin{aligned}
\frac{\partial\Delta\varphi_i}{\partial\zeta} &= -\frac{\Delta\beta_i z_{\text{eff}}}{1-\alpha z_{\text{eff}}\zeta} - \frac{1}{3}\left\{ \left[\frac{P_i}{P_0}\right]\left(\xi_{yi}^2 - \xi_{xi}^2\right)\left(1-\cos\left(2\Delta\varphi_i\right)\right) \right. \\
&\quad \left. + 4\sum_{j\neq i}\left[\frac{P_j}{P_0}\right]\left(\xi_{yj}^2 - \xi_{xj}^2\right) + 4\left[\frac{\xi_{xi}}{\xi_{yi}} - \frac{\xi_{yi}}{\xi_{xi}}\right]\cos\left(\Delta\varphi_i\right)\sum_{j\neq i}\left[\frac{P_j}{P_0}\right]\xi_{xj}\xi_{yj}\cos\left(\Delta\varphi_j\right) \right\} \qquad (16)
\end{aligned}$$

slow axis. Obviously, the separatrix can be decomposed into four segments. Two of them are circular arcs of the unit circle, whereas the other two are horizontal lines with distance

$$\sqrt{\frac{3}{2}\left|\Delta\beta\right| z_{\text{eff}}}$$

to the x–axis. Starting from states of polarization within the area shaded in light blue, the ellipticity will change sign during propagation. Since in the absence of absorption each state of polarization adopted during propagation can be considered as initial state and the process itself does not have a memory, the separatrix constitutes a borderline, that will not be crossed by any possible trace.

Figure 8 shows the polarization states adopted during propagation for a single initial state of polarization but variable magnitude of the birefrigence. Power exchange and evolution of the ellipticity are illustrated in figure 9. In this figure, the curves for $|\Delta\beta|\, z_{\text{eff}} = 10$ are not shown, since the period is in this case significantly smaller as compared to the other ones so that this curve would cover all the other ones.

The red curve shows the trace for $|\Delta\beta|\, z_{\text{eff}} = 0$, i. e. for vanishing birefrigence. It is the already presented curve with constant ellipticity. In case of the green curve, representing the trace for $|\Delta\beta|\, z_{\text{eff}} = 0.150$, the initial state of polarization is outside of the area encompassed by the separatrix. Thus, the orientation of rotation of the electrical field vector does not change during propagation and the trace on the Poincaré sphere is completely on the upper hemisphere. The other curves represent traces for $|\Delta\beta|\, z_{\text{eff}} > 1/6$, so that the initial state of polarization is within the area embraced by the separatrix. Therefore, the sign of the ellipticity changes periodically. For increasing values of $|\Delta\beta|\, z_{\text{eff}}$, the traces in the Jones based representation tend towards a circle. The traces on the Poincaré sphere also converge towards a cercle. It can be generated by rotating the initial state of polarization around the S_1–axis. The constant value of S_1 implies that there is no longer a power exchange between the two components of the Jones vector.

B. with attenuation

The influence of fiber attenuation becomes clear when considering the first term after the equals sign in equation (16). With increasing propagation diestance, the normalized effective length ζ tends towards its maximum value $1/(\alpha \cdot z_{\text{eff}})$. As a consequence, the denominator converges against zero, what can be interpreted as a continuous increase of the effective birefrigence

$$\Delta\beta_{\text{eff}} = \frac{\Delta\beta}{1-\alpha\cdot z_{\text{eff}}\cdot\zeta} \quad .$$

Therefore, the trace in the Jones based representation follows first the trace that has been determined for the case without fiber attenuation, but finally tends more and more towards a circle, as shown in figure 10. This implies, that the amount of power exchanged among the two components of the Jones vector decreases continuously and tends towards zero (see figure 11). The period length assigned to this power exchange also decreases with growing ζ, whereas it is constant if expressed in terms of the physical propagation distance z.

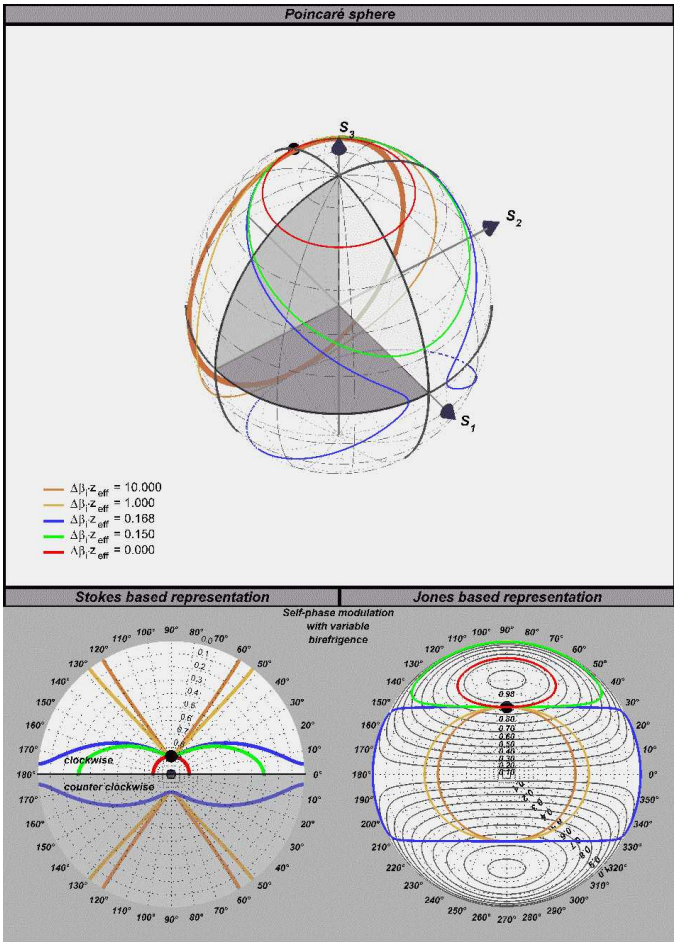

Fig. 8. Changes of the polarization state induced by self–phase modulation and birefrigence without fiber attenuation. The polarization state at the fiber input has been marked by a dot.

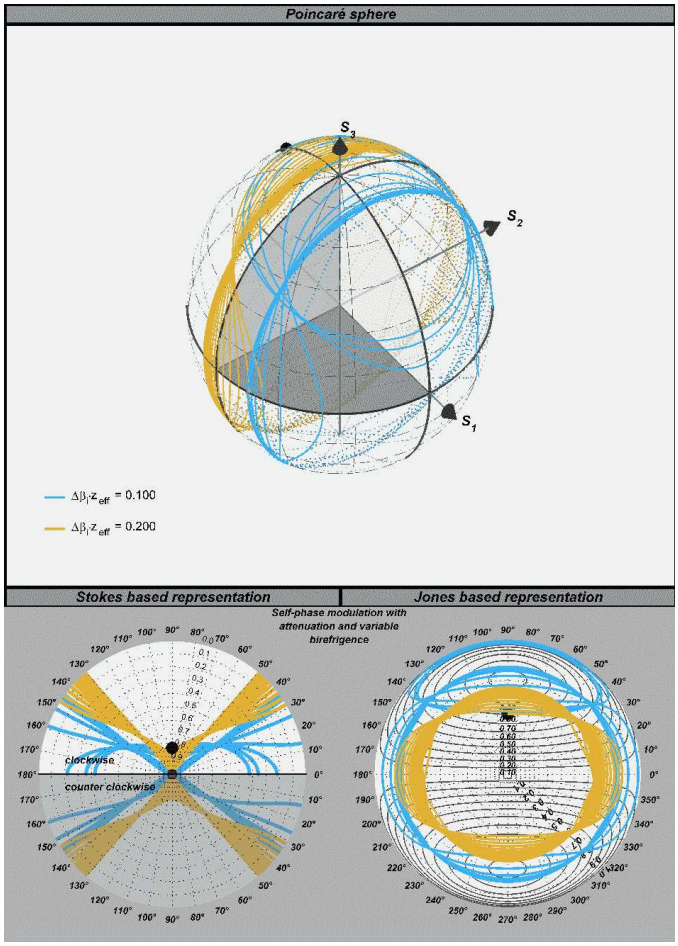

Fig. 10. Changes of the polarization state induced by self–phase modulation and birefrigence with fiber attenuation. The polarization state at the fiber input has been marked by a dot.

VI. The Effect of Cross–Phase Modulation

A. Cross–phase modulation only

The propagation of two channels with arbitrary polarization is investigated in order to study the effect of cross–phase modulation. One channel, named first channel in the following, is launched at power P_1 into the fiber, whereas the input power of the second channel is assumed to be negligible ($P_2 \approx 0$). In this way, there is no interaction between the two components of the second channel, but they are influenced by the first channel. Thus, the polarization of the second channel is altered by XPM only. Fiber attenuation will be neglected in this section.

Polarization changes of the first channel induced by SPM are visualized by the blue curve in figure 12. It is the curve with constant ellipticity. The structure of the polarization traces for the second channel is significantly more complex. In addition, this curve crosses the equator, separating the Poincaré sphere into an upper and lower hemisphere. Its shape depends on the initial polarizations of both channels. The traces shown in

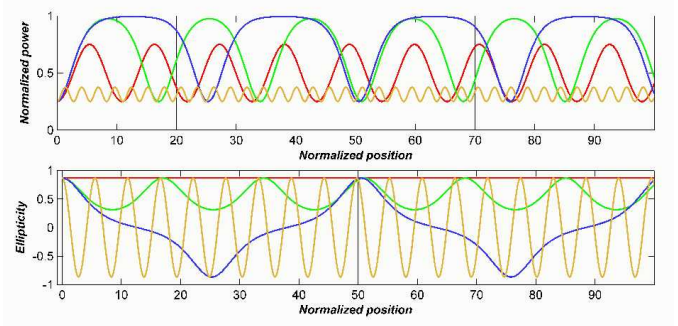

Fig. 9. Evolution of power in the x–axis and ellipticity versus normalized fiber position for different polarization states at the fiber input (no fiber attenuation, with birefrigence).

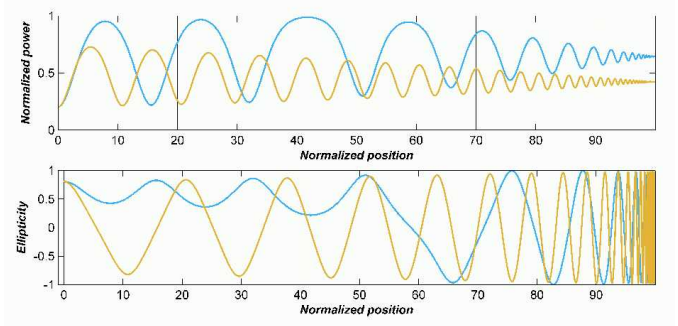

Fig. 11. Evolution of power in the x–axis and ellipticity versus normalized fiber position for different polarization states at the fiber input (with fiber attenuation, with birefrigence).

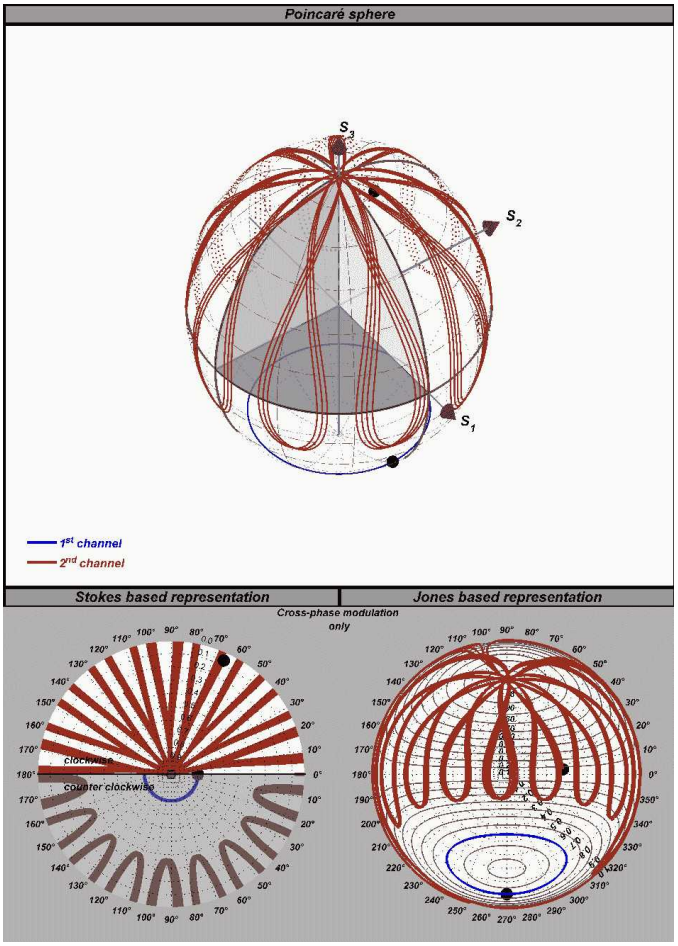

Fig. 12. Changes of the polarization state induced by cross–phase modulation without fiber attenuation and without birefrigence. The polarization state at the fiber input has been marked by a dot. Blue curve: channel at large input power, red curve: channel with negligible input power.

the Stokes based representation indicate that the magnitude of the ellipticity changes significantly faster than the direction of the polarization ellipse. The segments in the upper part of the diagram are very similar to the ray–like traces that we have already seen as a result of birefrigence (see Fig. 3). However, the significant difference is that the orientation does not change between two values, but rather changes in small steps.

As shown in figure 13, the ellipticity is a sinusoidal function

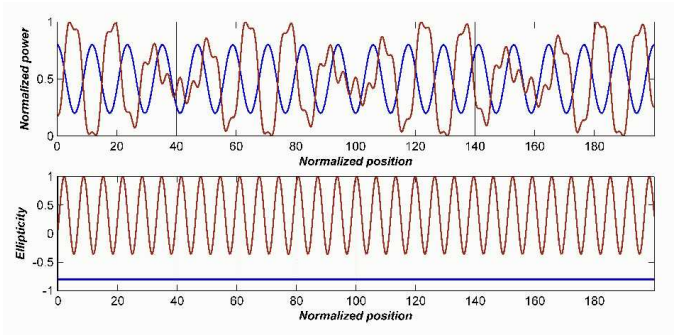

Fig. 13. Evolution of power in the x–axis and ellipticity versus normalized fiber position for different polarization states at the fiber input (without attenuation, without birefrigence). Blue curve: channel at large input power, red curve: channel with negligible input power.

of the normalized fiber position. It can be described by the equation

$$\begin{aligned} \varepsilon_2 &= 2\xi_{x2}\sqrt{1-\xi_{x2}^2}\sin\left(\Delta\varphi_2\right) \\ &= C_2 + \Delta\varepsilon_2 \cos\left(\frac{\zeta+\zeta_{02}}{\zeta_{c2}}\right) \quad . \end{aligned} \tag{18}$$

The period length

$$\zeta_{c2} = \frac{3}{4}\frac{1}{\sqrt{1-\frac{3}{4}\varepsilon_1^2}}\cdot\frac{P_0}{P_1} \tag{19}$$

is governed solely by the ellipticity of the first channel. It can be shown that the power of the x–component of the second channel can be described by

$$\begin{aligned} \mathcal{P}_{x2} &= \frac{1}{2} + \frac{4}{3}\left[\frac{P_1}{P_0}\right]\sqrt{1-\varepsilon_1^2}\Bigg\{ C_2\zeta_{c1}\sin\left(\frac{\zeta+\zeta_{01}}{\zeta_{c1}}\right) \\ &+ \frac{\Delta\varepsilon_2}{2}\frac{\zeta_{c1}\zeta_{c2}}{\zeta_{c2}+\zeta_{c1}}\sin\left(\frac{\zeta_{c2}+\zeta_{c1}}{\zeta_{c1}\zeta_{c2}}\zeta + \frac{\zeta_{01}}{\zeta_{c1}} + \frac{\zeta_{02}}{\zeta_{c2}}\right) \\ &+ \frac{\Delta\varepsilon_2}{2}\frac{\zeta_{c1}\zeta_{c2}}{\zeta_{c2}-\zeta_{c1}}\sin\left(\frac{\zeta_{c2}-\zeta_{c1}}{\zeta_{c1}\zeta_{c2}}\zeta + \frac{\zeta_{01}}{\zeta_{c1}} - \frac{\zeta_{02}}{\zeta_{c2}}\right) \quad . \end{aligned} \tag{20}$$

Obviously, the power of the x–component of the second channel versus normalized propagation distance ζ can be described by the superposition of a constant value and three sine functions with different period lengths. The average value of the power of each component equals one half. We astain here from describing the constants $\Delta\varepsilon_2$, C_2, and ζ_{02} in an analytical form. However, the peak–to–peak variation $2\Delta\varepsilon_2$ of the ellipticity of the second channel is illustrated in figures 14 and 15 versus the initial state of polarization of the first channel for two initial states of polarization of the first channel.

First, the case of linear polarization of the first channel at the input of the fiber is considered. According to figure 14, the XPM induced change of the ellipticity is minimum if the principal axis of the initial states of polarization of both channels are either oriented in identical directions or it they are orthogonal, whereas maximum variation occurs if the angle between both transverse axes equals $45° + N \times 90°$ with N being an entire number. The variation vanishes completely if the direction of the polarization of both channels is identical. In addition, the magnitude of the variation is independent of sign of the ellipticity.

A different behavior is observed if the first channel is elliptically polarized at the input of the fiber. Again, maximum variation is observed in case the angle between both principal axis equals $45° + N \times 90°$. Minimum variation also takes now place if the sign of the initial ellipticity is identical for both channels and the principal axes have the same direction or if the principal axis are orthogonal for different signs of the initial ellipticities. But the values of the two other local minimum are now significantly larger.

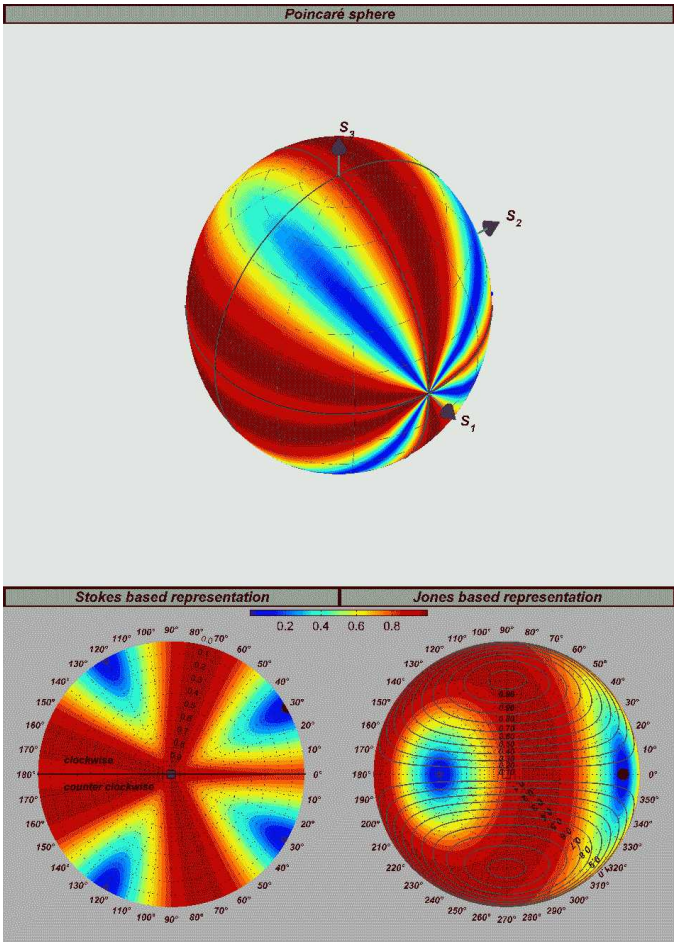

Fig. 14. Color coded plot showing the peak–to–peak variation of the ellipticity $2\Delta\varepsilon_2$ versus the initial state of polarization of the second channel induced by XPM only. The first channel is linearly polarized at the input of the fiber. The angle with the x–axis equals $30°$.

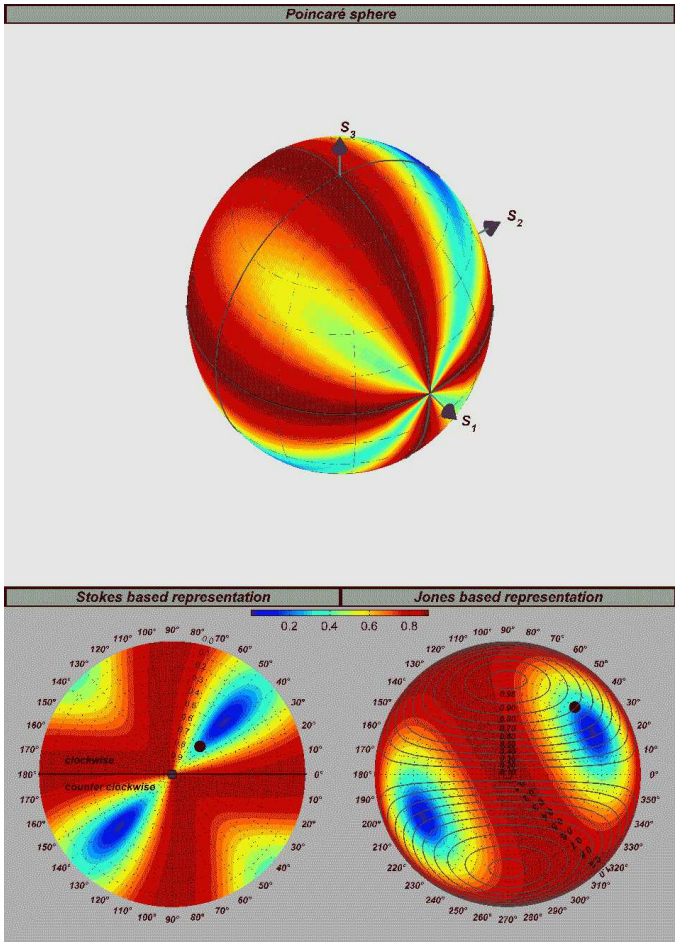

Fig. 15. Color coded plot showing the peak–to–peak variation of the ellipticity $2\Delta\varepsilon_2$ versus the initial state of polarization of the second channel. The first channel is elliptically polarized at the input of the fiber.

B. Combined with self–phase modulation

So far, the effect of cross–phase modulation without interaction with other effects has been studied. In order to investigate the interplay of self–phase modulation and cross–phase modulation, we will now assume that both interacting channels are launched at identical power into the fiber. The states of polarization of the first channel are found on the blue curves in Fig. 16, whereas the red line represents the trace of the polarization states of the second channel.

Not surprisingly, the shape of the traces is very similar for both channels. This statement is also valid with respect to the evolution of power and ellipticity versus fiber axes, as illustrated in Fig. 17. Both curves are periodic and the sum of the ellipticities of the curves is constant. This is in agreement with equation (12).

As before, the total variation of the ellipticity of the second channel has been determined for linear polarization of the first channel at the fiber input. As shown in Fig. 18, there are again four local minima in the Stokes based representation.

Corresponding results for elliptical polarization of the first channel at the fiber input are represented in Fig. 19. The most remarkable aspect of this representation is that the patterns in the two hemisphere are no longer identical. In contrast to the former cases, minimum variation only occurs if the electrical field vector of the second channel is rotating clockwise, as the electrical field vector of the first channel does. In contrast, maximum variation can only be achieved for contrarian senses of the rotation.

VII. Interplay of Cross–Phase Modulation and Birefrigence

Evolution of the state of polarization for the combined effect of XPM and birefrigence without fiber attenuation is shown in Fig. 20. The structure of the trace for the second channel is rather complex. However, there are still several segments where the magnitude of the ellipticity changes very rapidly, whereas the orientation of the polarization ellipse is rather constant. Power and ellipticity are shown in Fig. 21 versus normalized propagation distance for both channels. The two figures are periodic functions. For comparison purposes, the trace propagation in the presence of fiber attenuation is shown in Fig. 22.

Adding now the effect of SPM but neglecting again fiber attenuation, we get the plot shown in Fig. 23 for the magnitude

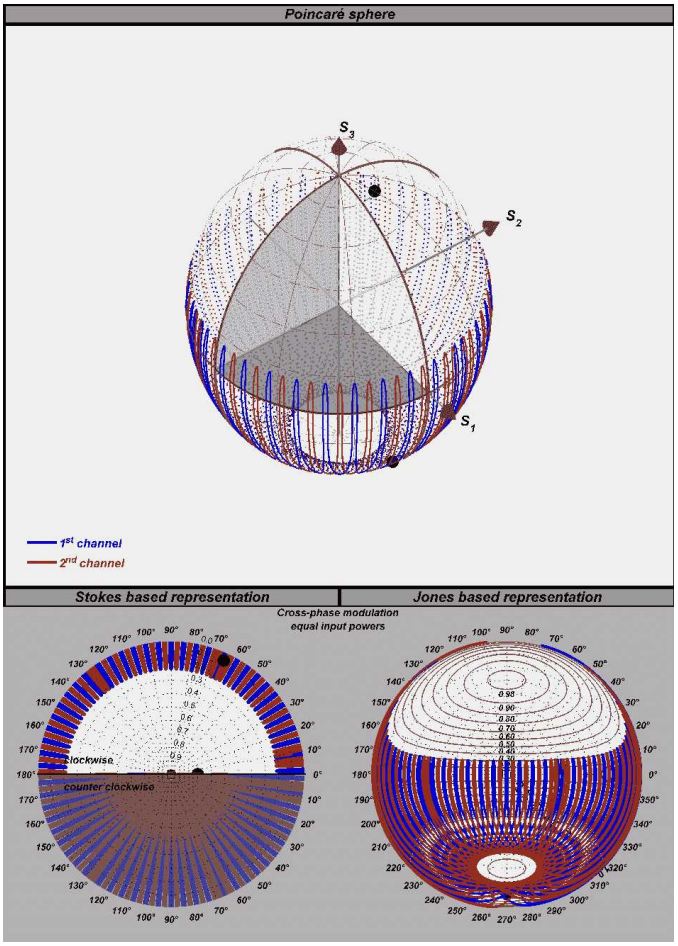

Fig. 16. Changes of the polarization state induced by cross–phase modulation without fiber attenuation and birefrigence. The polarization state at the fiber input has been marked by a dot. Both channels are launched at equal input power into the fiber.

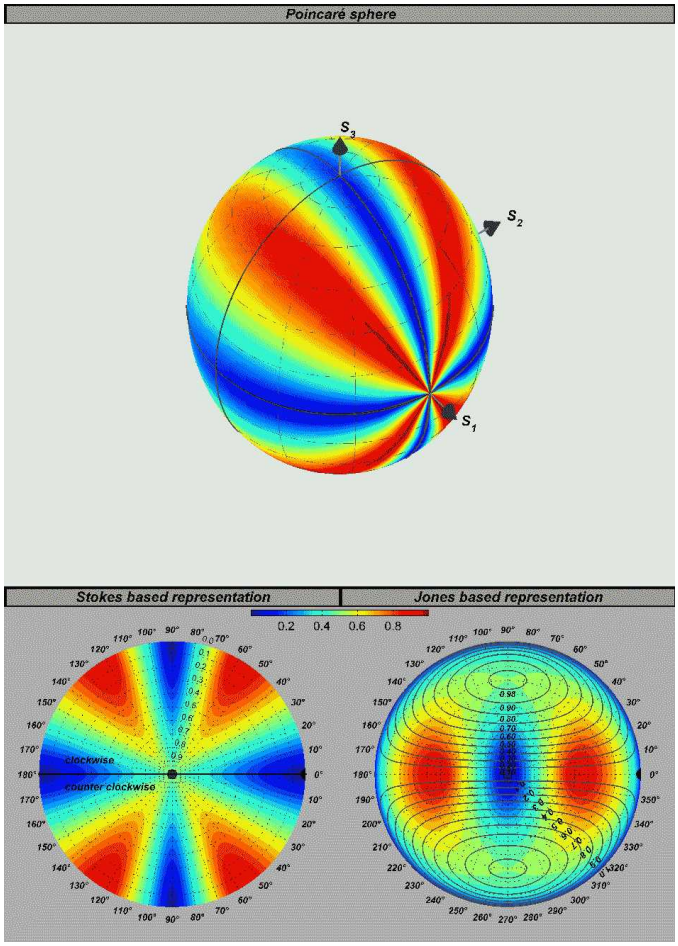

Fig. 18. Color coded plot showing the peak–to–peak variation of the ellipticity $2\Delta\varepsilon_2$ versus the initial state of polarization of the second channel induced by the interplay of SPM and XPM. The first channel is linearly polarized at the input of the fiber in direction of the x–axis.

of the changes of the ellipticity for elliptical polarization of the first channel at the fiber input. As compared with the illustration for the case without birefrigence in Fig. 19, the patterns are quite similar. However, deeply red areas cover a larger part of the total area in the Stokes based representation. In addition, there is now also an area with large magnitude of the variation of the ellipticity for identical sense of rotation.

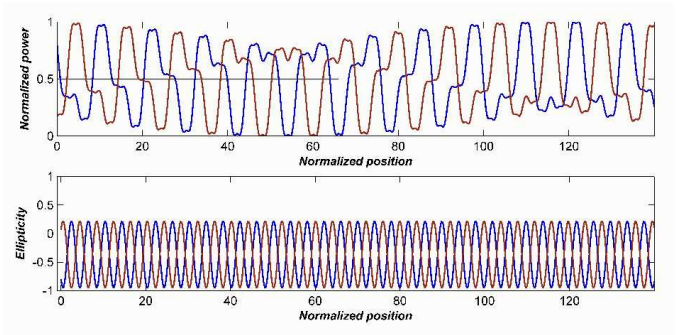

Fig. 17. Evolution of power in the x–axis and ellipticity versus normalized fiber position for different polarization states at the fiber input (without attenuation, without birefrigence). Both channels are launched at equal input power into the fiber.

VIII. Conclusion

The effect of self–phase modulation (SPM), cross–phase modulation (XPM) and birefrigence on the state of polarization has been investigated for continuous wave (cw) configurations.

Starting from the nonlinear Schrödinger equation, it has been shown that self–phase (SPM) modulation and cross–phase modulation (SPM) do not induce a power transfer among the channels of a wavelength division multiplexing (WDM) system. However, power is exchanged among the components of the Jones vector of the individual channels. Without attenuation, this power exchange is a periodic function of the propagation distance. Furthermore, the analysis revealed that the sum of the ellipticities weighted by the corresponding fiber input power is preserved during propagation as long as the wavelength dependence of fiber attenuation can be neglected and there is no birefrigence.

First, the effect of self–phase modulation without interaction of birefrigence has been investigated. It has been shown that the ellipticity of the channel under consideration is maintained during propagation even under the influence of SPM. In addition, the power of the different components of the Jones

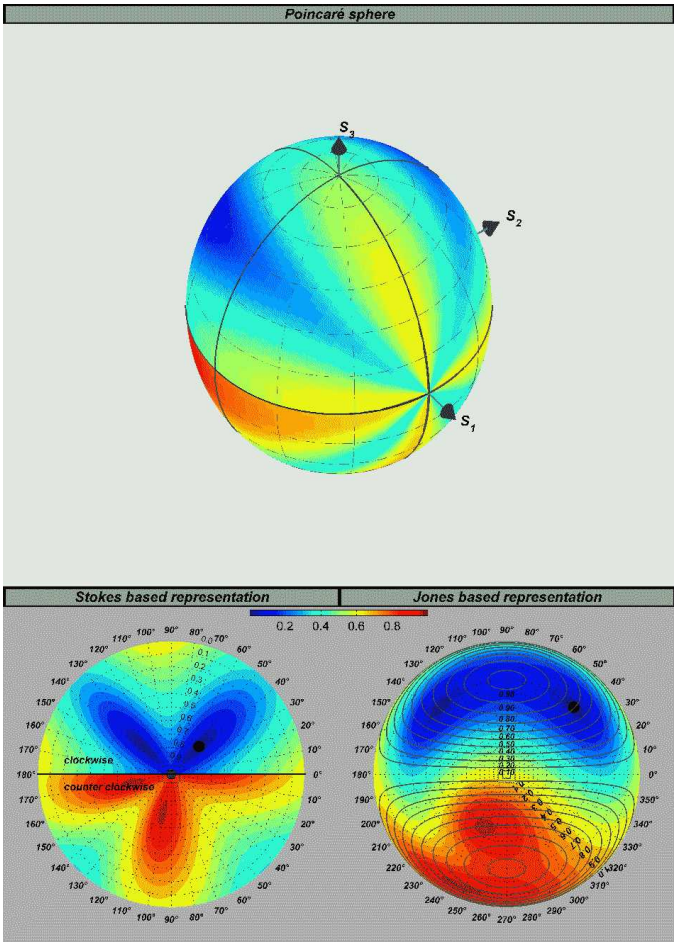

Fig. 19. Color coded plot showing the peak–to–peak variation of the ellipticity $2\Delta\varepsilon_2$ versus the initial state of polarization of the second channel induced by the interplay of SPM and XPM. The first channel is elliptically polarized at the input of the fiber.

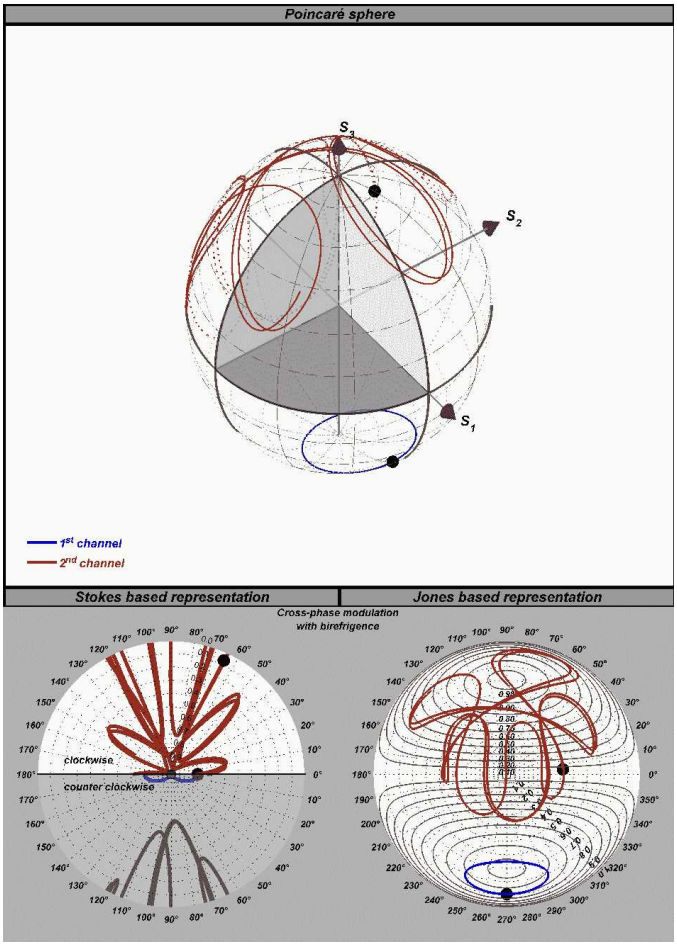

Fig. 20. Changes of the polarization state induced by cross–phase modulation without fiber attenuation, but with birefrigence. The polarization state at the fiber input has been marked by a dot.

vector change sinusoidally as a function of a normalized propagation distance. Closed–form expressions describing the dependence of the magnitude of the power variation and the period length on initial conditions at the fiber input have been derived. The results indicate that the state of polarization is not affected by SPM for the special cases of linear and circular polarization at the fiber input. When averaging over complete periods, the average power is identical for both components of the Jones vector.

Conservation of the ellipticity is canceled out by the interaction with birefrigence. Neglecting fiber attenuation, a different quantity has been identified that is conserved during propagation. Ellipticity as well as the power of the two components of the Jones vector change periodically versus propagation distance, but no longer sinusoidally. Furthermore, it has been shown that there is a separatrix that cannot be crossed by the traces embracing the states of polarization adopted during propagation. Thus, the Poincaré sphere is split into up to three segments. With fiber attenuation, the separatrix does no longer represent a fix borderline and the magnitude of the power exchange decreases continuously with propagation.

To determine the effect of cross–phase modulation (XPM) without interference of other effects, a configuration with a first channel launched at high power into the fiber and a second channel with small input power has been analyzed. The ellipticity of the low–power channel shows a sinusoidal dependence on the normalized propagation distance with a period length depending on the ellipticity of the first channel only. Power variation of both components of the Jones vector of the second channel can be mathematically described by a superposition of three sine waves. For elliptical and linear polarizations at the fiber input, maximum variation of the ellipticity is observed if the angle between the principal axis of the polarization ellipses of both channels equals approximately

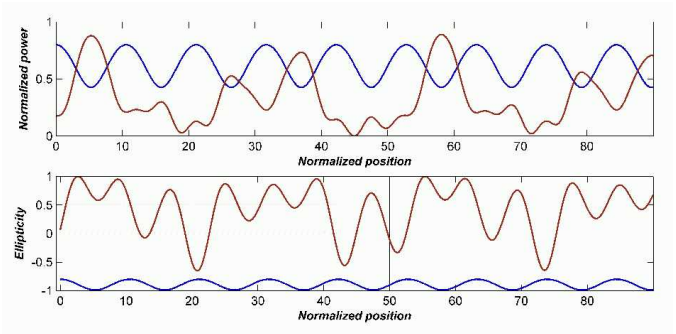

Fig. 21. Evolution of power in the x–axis and ellipticity versus normalized fiber position for different polarization states at the fiber input.

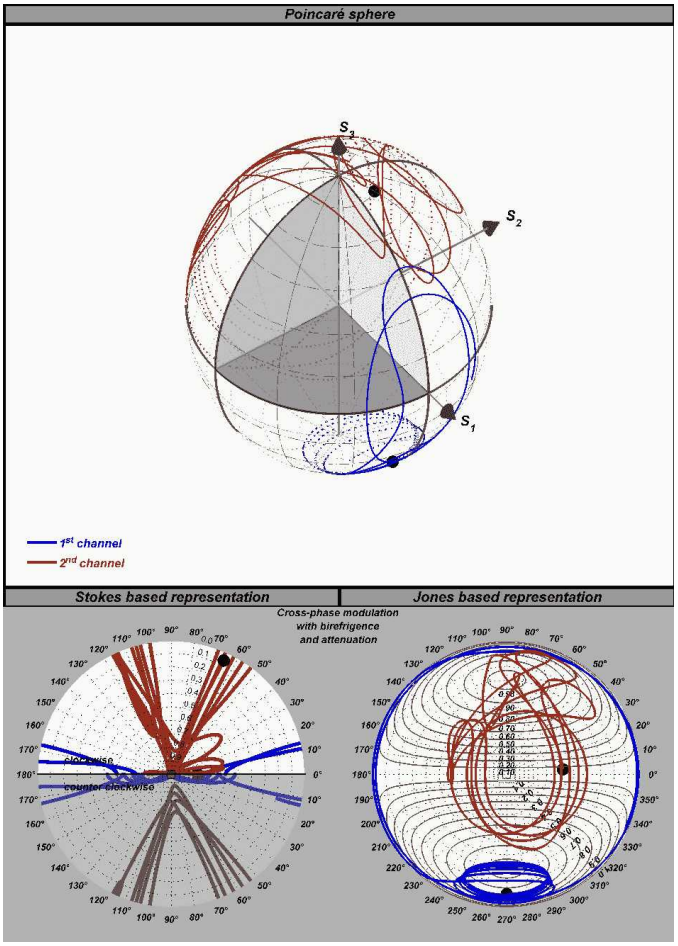

Fig. 22. Changes of the polarization state induced by cross–phase modulation with fiber attenuation and birefrigence. The polarization state at the fiber input has been marked by a dot.

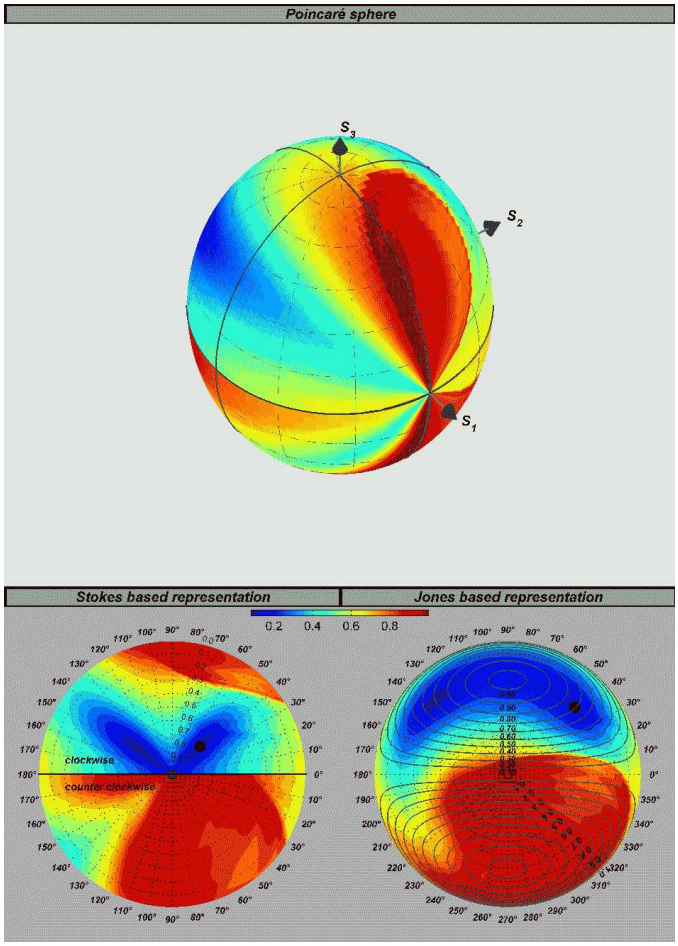

Fig. 23. Color coded plot showing the peak–to–peak variation of the ellipticity $2\Delta\varepsilon_2$ versus the initial state of polarization of the second channel induced by the interplay of SPM and XPM in the presence of birefrigence ($\Delta\beta \cdot z_{\text{eff}} = 0.15$). The first channel is elliptically polarized at the input of the fiber.

$45° + N \times 90°$ with N being an entire number.

Launching both channels at identical powers into the fiber gives rise to interaction of SPM and XPM. In case of linear polarization of the first channel at the fiber input, maximum variation of the ellipticity is observed if the angle between the principal axis of the polarization ellipses of both channels equals approximately $45° + N \times 90°$. However, in case of elliptical polarization of the first channel at the fiber input, it has been shown that — at least in some cases — maximum variation of the ellipticity can now only be achieved if the rotation senses of both channels are contrarian. If small birefrigence is added, the fundamental behavior does not change, but the relative portion of initial polarization states leading to large variation of the ellipticity increases.

IX. Appendix

Birefrigence leads to a wave–vector mismatch. In the frequently used representation of the coupled nonlinear Schrödinger equations [31], the effect of phase mismatch on the nonlinear interaction is taken into account by a factor $e^{\pm \jmath 2\Delta\beta_i z}$ multiplied with the product of three slowly varying amplitudes. This factor does not appear in equation (15). However, we will show in this section that the two representations are equivalent.

To simplify representation, the case of self–phase modulation only will be considered. In this case, equation (15) takes the form

$$\begin{aligned}\frac{\partial u_x}{\partial z} - \jmath\frac{\Delta\beta}{2}u_x &= -\jmath\frac{e^{-\alpha z}}{z_{\text{eff}}}\left\{u_x\left[|u_x|^2 + \frac{2}{3}|u_y|^2\right] + \frac{1}{3}u_x^* u_y^2\right\}\\ \frac{\partial u_y}{\partial z} + \jmath\frac{\Delta\beta}{2}u_y &= -\jmath\frac{e^{-\alpha z}}{z_{\text{eff}}}\left\{u_y\left[|u_y|^2 + \frac{2}{3}|u_x|^2\right] + \frac{1}{3}u_x^* u_y^2\right\} \quad . \qquad (21)\end{aligned}$$

The normalized complex amplitudes u_x and u_y stem from the representation

$$E_x(\tau, z) = \Re\left\{E_x^{(0)}\Psi_x(x,y)u_x(\tau,z)\cdot \exp\left(-\frac{\alpha}{2}z\right)\exp\left(\Omega\tau - \jmath\bar{\beta}^{(0)}z\right)\right\}$$

$$E_y(\tau,z) = \Re\Big\{E_y^{(0)}\Psi_y(x,y)u_y(\tau,z)\cdot \exp\left(-\frac{\alpha}{2}z\right)\exp\left(\Omega\tau-\jmath\bar{\beta}^{(0)}z\right)\Big\} \quad (22)$$

for the two components of the electrical field, where $\Re$ stands for the real part of the argument in brackets. The constant $E^{(0)}$ accounts for the initial electrical field at the fiber input, Ω stands for the angular frequency, and the modal field distribution is represented by Ψ. The important difference to the usually employed mathematical description is that there is a common mode–propagation constant

$$\bar{\beta}^{(0)} = \frac{\beta_x^{(0)}+\beta_y^{(0)}}{2} \quad (23)$$

used for both waves. It is defined as the average of the propagation constants $\beta_x^{(0)}$ and $\beta_y^{(0)}$ for the two components. In this way, the differences with respect to the propagation constant affect directly the complex amplitudes u_x and u_y.

However, it is also possible to define the complex amplitudes for the different waves with respect to their respective mode–propagation constants. This approach is very suitable if the evolution of lightwaves is considered separately. However, the determination of the state of polarization is more difficult. The electrical field components are now given by

$$E_x(\tau,z) = \Re\Big\{E_x^{(0)}\Psi_x(x,y)U_x(\tau,z)\cdot \exp\left(-\frac{\alpha}{2}z\right)\exp\left(\Omega\tau-\jmath\beta_x^{(0)}z\right)\Big\}$$

$$E_y(\tau,z) = \Re\Big\{E_y^{(0)}\Psi_y(x,y)U_y(\tau,z)\cdot \exp\left(-\frac{\alpha}{2}z\right)\exp\left(\Omega\tau-\jmath\beta_y^{(0)}z\right)\Big\} \quad (24)$$

with the normalized complex amplitudes U_x and U_y, which are again related by the equations

$$u_x = U_x\cdot e^{-\jmath\frac{\Delta\beta}{2}z} \quad (25)$$

$$u_y = U_y\cdot e^{\jmath\frac{\Delta\beta}{2}z} \quad (26)$$

to the normalized amplitudes used before. As before, the parameter

$$\Delta\beta = \beta_x^{(0)}-\beta_y^{(0)}$$

denotes the difference of the propgation constants. Substituting u_x and u_y in equation (21) by making use of these relations gives

$$\frac{\partial U_x}{\partial z} = -\jmath\frac{e^{-\alpha z}}{z_{\text{eff}}}\left\{U_x\left[|U_x|^2+\frac{2}{3}|U_y|^2\right]+\frac{1}{3}U_x^*U_y^2\underbrace{e^{\jmath 2\Delta\beta_i z}}_{\mathcal{PM}_{\mathcal{A}}}\right\}$$

$$\frac{\partial U_y}{\partial z} = -\jmath\frac{e^{-\alpha z}}{z_{\text{eff}}}\left\{u_y\left[|U_y|^2+\frac{2}{3}|U_x|^2\right]+\frac{1}{3}U_x^*U_y^2\cdot\underbrace{e^{-\jmath 2\Delta\beta_i z}}_{\mathcal{PM}_{\mathcal{B}}}\right\} \quad (27)$$

where the efect of the phase mismatch due to birefrigence is introduced by the terms $\mathcal{PM}_{\mathcal{A}}$ and $\mathcal{PM}_{\mathcal{B}}$ in the well–known way used in [31].

REFERENCES

[1] D. Lee, *Electromagnetic Principles of Integrated Optics*, John Wiley & Sons, New York, 1986.

[2] G. Einarsson, *Principles of Lightwave Communications*, John Wiley & Sons, Chichester, 1996.

[3] I. P. Kaminow, "Polarization in optical fibers," *IEEE J. Quant. El.*, vol. 17, no. 1, pp. 15–22, Jan. 1981.

[4] L. E. Nelson and R. M. Jopson, "Introduction to polarization mode dispersion in optical systems," in *Polarization Mode Dispersion*, A. Galtarossa and C. R. Menyuk, Eds., pp. 1–27. Springer, New York, 2005.

[5] H. Xu, B. S. Marks, J. Zweck, L. Yan, C. R. Menyuk, and G. M. Carter, "Statistical properties of the DGD in a long–haul optical fiber with temporally drifting birefrigence," *IEEE J. Lightw. Technol.*, vol. 24, no. 3, pp. 1165–1175, Mar. 2006.

[6] J. P. Gordon and H. Kogelnik, "PMD fundamentals: Polarization mode dispersion in optical fibers," *Prodeedings of the National Academy of Sciences of the USA*, vol. 97, no. 9, pp. 4541–4550, Feb. 2000.

[7] J. Zhou and M. J. O'Mahony, "Optical transmission system penalties due to fiber polarization mode dispersion," *IEEE Photon. Technol. Lett.*, vol. 6, no. 10, pp. 1265–1267, Oct. 1994.

[8] H. Bülow and S. Lanne, "PMD compensation techniques," in *Polarization Mode Dispersion*, A. Galtarossa and C. R. Menyuk, Eds., pp. 225–245. Springer, New York, 2005.

[9] M. Jäger, T. Rankl, J. Speidel, H. Bülow, and F. Buchali, "Performance of turbo equalizers for optical PMD channels," *IEEE J. Lightw. Technol.*, vol. 24, no. 3, pp. 1226–1236, Mar. 2006.

[10] L. Chen, S. Hadjifaradji, and X. Bao, "Analytic optical eye diagram evaluation in the presence of polarization–mode dispersion, polarization–dependent loss, and chromatic dispersion in dynamic single mode fiber communication networks," *J. Opt. Soc. Am. B*, vol. 21, no. 10, pp. 1860–1865, Oct. 2004.

[11] Q. Yu and C. Fan, "Analytical study on pulse broadening in chained optical amplifier systems," *IEEE J. Lightw. Technol.*, vol. 15, no. 3, pp. 444–451, Mar. 1997.

[12] N. Kikuchi and S. Sasaki, "Analytical evaluation technique of self–phase–modulation effect on the performance of cascaded optical amplifier systems," *IEEE J. Lightw. Technol.*, vol. 13, no. 5, pp. 868–878, May 1995.

[13] T.-K. Chiang, N. Kagi, T. K. Fong, M. E. Marhic, and L. G. Kazovsky, "Cross–phase modulation in dispersive fibers: Theoretical and experimental investigation of the impact of modulation frequency," *IEEE Photon. Technol. Lett.*, vol. 6, no. 6, pp. 733–737, June 1994.

[14] A. R. Chraplyvy, "Limitations on lightwave communications imposed by optical–fiber nonlinearities," *IEEE J. Lightw. Technol.*, vol. 8, no. 10, pp. 1548–1557, Oct. 1990.

[15] L. Rapp, "Experimental investigation of signal distortions induced by cross–phase modulation combined with dispersion," *IEEE Photon. Technol. Lett.*, vol. 9, no. 12, pp. 1592–1594, Dec. 1997.

[16] K. Inoue, "Experimental study on channel crosstalk due to fiber four–wave mixing around the zero–dispersion wavelength," *IEEE J. Lightw. Technol.*, vol. 12, no. 6, pp. 1023–1028, June 1994.

[17] E. Lichtman, "Performance degradation due to four–wave mixing in multichannel coherent optical communications systems," *Journ. Opt. Comm.*, vol. 12, no. 2, pp. 53–58, 1991.

[18] F. Matera and M. Settembre, "Compensation of polarization mode dispersion by means of Kerr effect for nonreturn–to–zero signals," *Optics Letters*, vol. 20, no. 1, pp. 28–30, Jan. 1995.

[19] E. Corbel, J. P. Thiéry, S. Lanne, and S. Bigo, "Experimental statistical assessment of XPM impact on optical PMD compensator efficiency," in *Proc. Optical Fiber Communication Conference*, Atlanta, USA, March 2003, pp. 499–501.

[20] L. Bononi and L. Barbieri, "Design of gain–clamped doped–fiber amplifiers for optical dynamic performance," *IEEE J. Lightw. Technol.*, vol. 17, no. 7, pp. 1229–1240, July 1999.

[21] A. Vannucci, A. Bononi, A. Orlandini, E. Corbel, J. Thiéry, S. Lanne, and S. Bigo, "A simple formula for the degree of polarization degraded by XPM and its experimental validation," in *Proc. Optical Fiber Communication Conference*, Atlanta, USA, March 2003, pp. 498–499.

[22] B. C. Collings and L. Boivin, "Nonlinear polarization evolution induced by cross–phase modulation and its impact on transmission systems," *IEEE Photon. Technol. Lett.*, vol. 12, no. 11, pp. 1582–1584, Nov. 2000.

[23] C. R. Menyuk and B. S. Marks, "Interaction of polarization mode dispersion and nonlinearity in optical fiber transmission systems," *IEEE J. Lightw. Technol.*, vol. 24, no. 7, pp. 2806–2826, July 2006.

[24] Q. Lin and G. P. Agrawal, "Effects of polarization–mode dispersion on cross–phase modulation in dispersion–managed wavelength–division–multiplexed systems," *IEEE J. Lightw. Technol.*, vol. 22, no. 4, pp. 977–987, Apr. 2004.

[25] Q. Lin and G. P. Agrawal, "Vector theory of cross–phase modulation: Role of nonlinear polarization rotation," *IEEE J. Lightw. Technol.*, vol. 40, no. 7, pp. 958–964, July 2004.

[26] N. Hanik, "Influence of polarisation mode dispersion on the effect of cross phase modulation in optical WDM transmission," in *Intern. Conf. Trans. Opt. Networks*, Wroclaw, Poland, July 2004, pp. 190–194.

[27] N. Hanik, "Modelling of nonlinear optical wave propagation including linear mode–coupling and birefrigence," *Optical Comm.*, vol. 214, pp. 207–230, 2002.

[28] C. Heras, J. M. Subías Domingo, J. Pelayo, and F. Villuendas, "Polarization properties of optical spectral components generated by XPM effect," *IEEE J. Lightw. Technol.*, vol. 25, no. 5, pp. 1313–1321, May 2007.

[29] D. Wang and C. R. Menyuk, "Polarization evolution due to the Kerr nonlinearity and chromatic dispersion," *IEEE J. Lightw. Technol.*, vol. 17, no. 12, pp. 2520–2529, Dec. 1999.

[30] S. Huard, *Polarization of Light*, Wiley, Chichester, 1997.

[31] G. P. Agrawal, *Nonlinear Fiber Optics*, Academic Press, San Diego, 4 edition, 2007.